Chapter

Cholesteric Liquid Crystal Polyesteramides: Non-Viral Vectors

Mercedes Pérez Méndez and José Fayos Alcañiz

Abstract

Polyesteramides PNOBDME $(C_{34}H_{38}N_2O_6)_n$, Poly[oxy(1,2-dodecane)-oxy-carbonyl-1,4-phenylene-amine-carbonyl-1,4-phenylene-carbonyl-amine-1,4-phenylene-carbonyl], and PNOBEE $(C_{26}H_{22}N_2O_6)_n$, Poly[oxy(1,2-butylene)-oxy-carbonyl-1,4-phenylene-amine-carbonyl-1,4-phenylene-carbonyl-amine-1,4-phenylene-carbonyl], have been designed and synthesized as cholesteric liquid crystals (LCs)—through a condensation reaction between 4- 4′-(terephthaloyl-diaminedibenzoic chloride) (NOBC) and racemic glycol, DL-1,2-dodecanediol or DL-1,2-butanediol, respectively—as chemical modifications of multifunctional cholesteric LC polyesters, involving new properties but holding the precursor helical macromolecular structures. The new compounds have been characterized by ^{1}H and ^{13}C-NMR, COSY and HSQC, exhibiting two ^{1}H-independent sets of signals observed for each enantiomer, attributed to two diastereomeric conformers, *gg* and *gt*, of the torsion containing the asymmetric carbon atom in the spacer. They have also been characterized by x-ray diffraction with synchrotron radiation source. Thermal behaviour of the new compounds is studied by thermogravimetric (TG) and differential scanning calorimetry (DSC) analysis. The substitution of the ester groups in the mesogen by amide groups causes an increase of thermal stability with respect to the precursors. Optical rotatory dispersion (ORD) is evaluated. Morphology of powdered PNOBDME exhibits spherical clusters of about 5 μm in diameter homogeneously dispersed. Molecular models show helical polymeric chains with stereoregular head-tail, isotactic structure, explained as due to the higher reactivity of the primary hydroxyl with respect to the secondary one in the glycol through the polycondensation reaction. Besides being biocompatible, these synthetic polyesteramides have proved to act as non-viral vectors in gene therapy and be able to transfect DNA to the nucleus cell. Similar new cationic cholesteric liquid crystal polyesters have also been synthesized in our laboratory.

Keywords: cholesteric LC polymer, biocompatible polyesteramides, synthesis, characterization, SAXS/WAXS, molecular simulation

1. Introduction

In 1944, Erwin Schrödinger, one of the founders of quantum mechanics, completed in Dublin a small book entitled *What Is Life? The Physical Aspect of the Living Cell* [1]. He predicted there the concept of "aperiodic crystal", to define a gene or perhaps the whole fibre of the chromosome, "that in my opinion, is the material

carrier of life...," "able to grow in aggregates bigger and bigger without the clumsy resource of repetition in three directions" as crystals do [2].

The concept of "aperiodic crystal" was surprisingly premonitory 9 years before the structure of DNA fibres was determined by x-ray diffraction as a helical structure by Franklin [3] ("Photograph 51" in **Figure 1(a)**), Wilkins [5] and Watson and Crick who reported the double helix with periodic order along the sugar-phosphate helical backbone, every 34 Å, and with the *aleatory* distribution of the complementary base pairs [4] (**Figure 1(b)**). The sequence of base pairs along the structure, without lateral periodic order, being convenient to endow DNA of their capacity to store genetic information.

In 1988 Ringsdorf evidenced the parallelism between thermotropic and lyotropic liquid crystals (LCs) in materials science and lipids in life science, with common amphiphilic nature [6]. Both self-organize their molecules in supramolecular systems, leading to functional units in highly oriented systems, exhibiting new properties. The importance of lyotropic LCs for the life sciences has been known for a long time as a prerequisite for the development of life and the ability of cells to function. In materials sciences, the concept of function through organization led to the development of new liquid crystalline materials for advanced applications.

Since 1992 the International Union of Crystallography redefined the concept of crystal as: "Any solid which has a diffraction pattern essentially discrete" (Fourier space) [7]. Since then, the *crystal family* was accepted to be composed of *periodic* and *aperiodic crystals*, and liquid crystals belong to the last group.

With increasing temperature, they do not directly go from the crystalline state into the melt, but, in the middle, they undergo a *mesophase* state which combines the order of perfect crystals and mobility of liquids.

All mesophases exhibit long-range orientational order, by keeping the parallel orientation of their longitudinal molecular axes. Two major classes can be

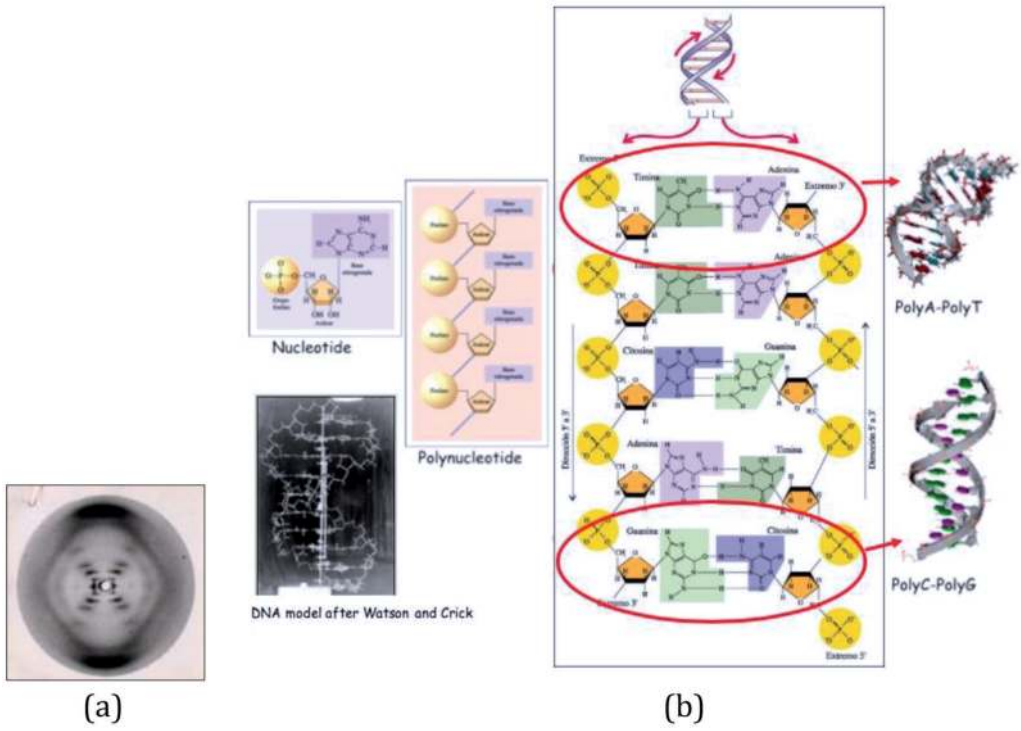

Figure 1.
(a) Photograph 51 by [3]; (b) DNA crystal structure according to [4]. Details of double-stranded PolyA-PolyT and PolyC-PolyG are shown at the right-hand side.

differentiated: *nematic* (with molecular centres distributed isotropically) and *smectic* (with their molecular centres organized in layers). The special array of nematic planes stacked in a helical superstructure with a prevalent screw direction is called the cholesteric mesophase (**Figure 2**).

DNA behaves as liquid crystal with the special array of the nematic planes, containing complementary base pairs, stacked in a superstructure with chiral helical symmetry of the charge distribution [8–10]. **Figure 3** shows micrographs of the cholesteric mesophase of DNA as the columnar hexagonal phase.

1.1 Synthetic cholesteric liquid crystal polymers

Two multifunctional cholesteric liquid crystal polyesters (ChLCP), named PTOBDME $[C_{34}H_{36}O_8]_n$ and PTOBEE $[C_{26}H_{20}O_8]_n$, with chemical formulations in **Figure 4**, were synthesized in our laboratory—through a condensation reaction between 4-4′-(terephthaloyl-dioxybenzoylchloride) (TOBC) and racemic glycol, DL-1,2-dodecanediol or DL-1,2-butanediol, respectively.

Although only racemic materials were used in their synthesis, a cholesteric, chiral morphology, theoretically unexpected, was found for PTOBDME, m = 9 in **Figure 4**. Evidence of this was obtained when a white solid, recrystallized as the second fraction from toluene mother liquor after the filtration of the polymer, was identified as –PTOBDME, with $[\alpha]^{25}_{589} = -1.43$ (1.538 g/100 ml, toluene). A similar result had been previously attained for liquid crystal PTOBEE, m = 1 in **Figure 4**. Its second fraction was isolated as –PTOBEE, with a value of $[\alpha]^{25}_{589} = -2.33$ (0.0056 mol/l, toluene). The synthetic method [11, 12], based on the previously reported by Bilibin [13, 14], leads to the obtaining of two or more fractions with progressively enriched diastereomeric excess. Its structure and diastereomeric excess could be characterized by NMR [15].

The structure of these optically active cholesteric LC polymers was characterized by NMR, Raman spectroscopy, steady-state fluorescence and SAXS/WAXS [16, 17], as rigid or semirigid helical LC polymers chains with flexible branches (chiral groups are located in the backbone), **Figure 5**, one of the major types of macromolecules forming the cholesteric mesophase [18].

Both polymers behave as thermotropic and lyotropic. They self-assemble in nanocavities in solution, with different conformations depending on the solvent

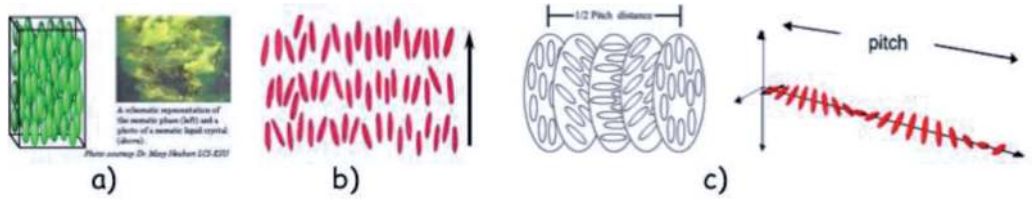

Figure 2.
Types of liquid crystal mesophases: (a) nematic, (b) smectic a and (c) cholesteric, helical pitch.

Figure 3.
Cholesteric mesophase of liquid crystal DNA exhibiting columnar hexagonal phase.

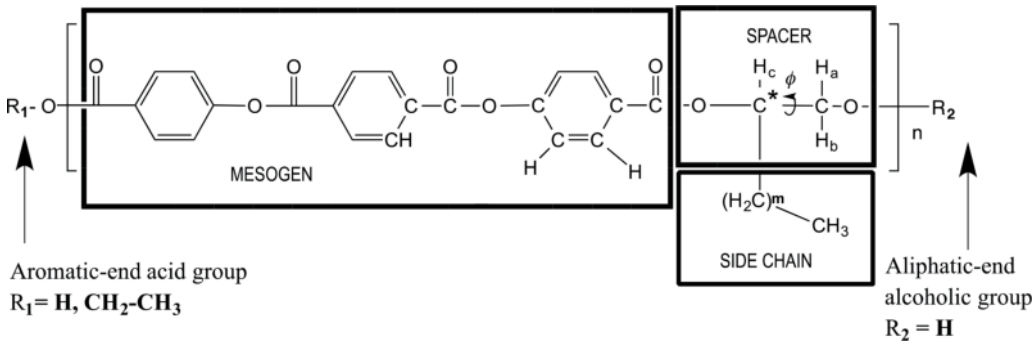

Figure 4.
The monomeric unit of cholesteric liquid crystal polyesters PTOBEE (m = 1) and PTOBDME (m = 9). The three different zones of the monomer are indicated: mesogen, spacer *and* flexible side chain. *The chiral Centre is indicated by an asterisk. Torsion ϕ is shown. The aromatic-end acid and aliphatic-end alcoholic groups are also shown.*

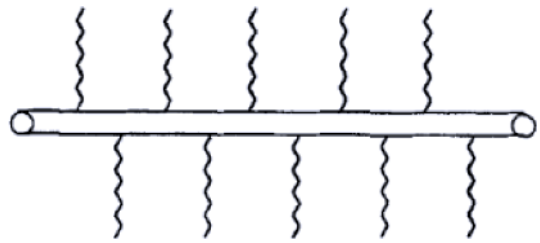

Figure 5.
Schematic representation of the cholesteric LC polymer type, with a rigid or semirigid helical chain with flexible branches (chiral groups are located in the backbone).

and on the concentration [16]. They also get adsorbed on metal surfaces with reordering of the polymer in the interface [19], with a potential application on the biomedical and engineering field.

Besides they have proved to be biocompatible against macrophages and fibroblasts cellular lines. They are also able to interact with biomacromolecules: lipids (neutral and cationic), polynucleotides and nucleic acids.

1.2 Interaction with lipids

Figure 6 shows liposomes of L-α-DMPC when interacting with cholesteric liquid crystal polyester PTOBDME, adopting hexagonal form. The structures of the lipid membranes complexed with cholesteric LC polymer were analysed by simultaneous SAXS/WAXS with synchrotron radiation source with λ = 1.5 Å on the X33

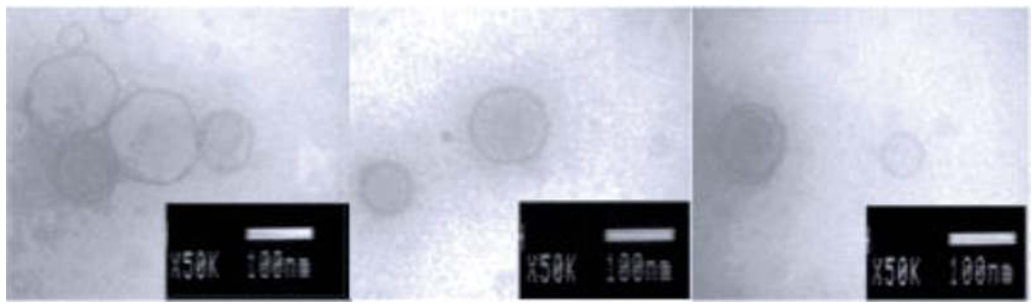

Figure 6.
TEM images of L-α-DMPC hexagonal liposomes complexed with PTOBDME.

camera at EMBL (DESY, Hamburg) [20–22]. Tripalmitin was used to calibrate both linear detectors. All data were normalized for incident intensity and analysed with Primus (ATSAS) [23, 24].

1.3 Interaction with polynucleotides and nucleic acids: non-viral vectors

The entrance of exogenous genetic material in cells was a key stage in the development of cellular biology. The term "transfection" indicates the transfer of DNA—as a healing agent—into the nuclei of cells of higher organisms. The direct application of this technology in living organisms opened crucial possibilities, like gene therapy and DNA vaccines [25].

Synthetic molecules that can bind polynucleotide fragments (the therapeutic agent) are required to develop new non-viral vectors to transfect in cells, without stimulating an immune response.

Cationic polymers, at physiological pH, are used to condense anionic nucleic acids, through self-assembly driven by electrostatic interactions, into nano-sized complexes called "polyplexes." DNA molecules being compressed to a relatively smaller size able to enter inside the nuclei of cells, facilitating internalization, thus improving transfection efficacy [26].

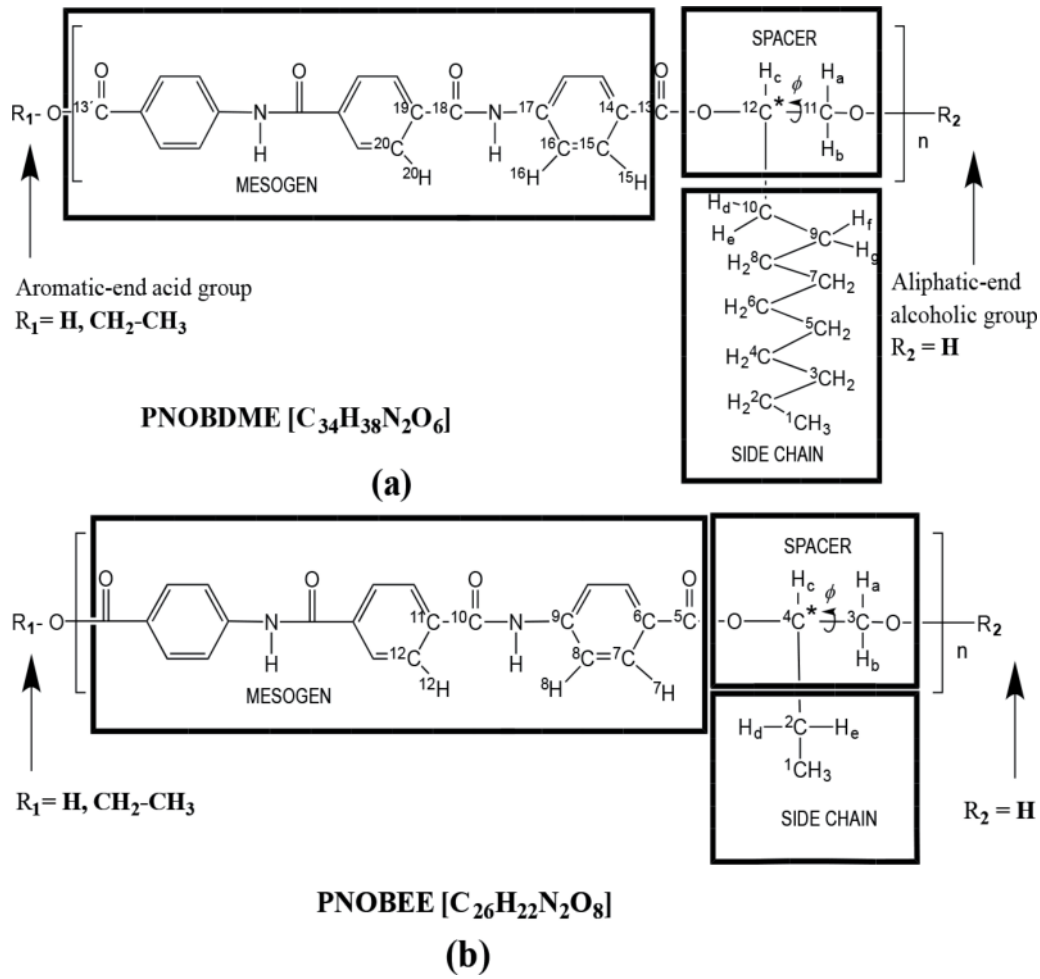

Figure 7.
The monomeric unit of polyesteramides: (a) PNOBDME; (b) PNOBEE. The asterisk indicates the chiral centre ($^{12}C^*$) in PNOBDME and ($^4C^*$) in PNOBEE. Torsion angle φ, along the ^{11}C–$^{12}C^*$ bond and ^3C–$^4C^*$ bond, respectively, is indicated.

New polyplexes were formulated including cholesteric LC PTOBDME and/or PTOBEE and *new monomeric cationic surfactant molecules* synthesized in our lab to entrap an anionic DNA plasmid. The new polyplexes successfully transfected both in vitro and in vivo in mice, as non-viral vectors for gene therapy. Their structures were studied by synchrotron radiation source [22, 27, 28].

New cationic chemical formulations of multifunctional cholesteric LCs PTOBDME and PTOBEE were designed later to directly interact with negatively charged DNA. The functional groups selected to be introduced at the end of the main polyester chains were choline [$–CH_2–CH_2–N^+–(CH_3)_3$] and ammonium, defined as [$–CH_2–CH_2–CH_2–N^+H–(CH_3)_2$]. Two more new polymers were also formulated with amide groups ($–CONH_2$) chemically bonded to the end of the lateral hydrophobic chains.

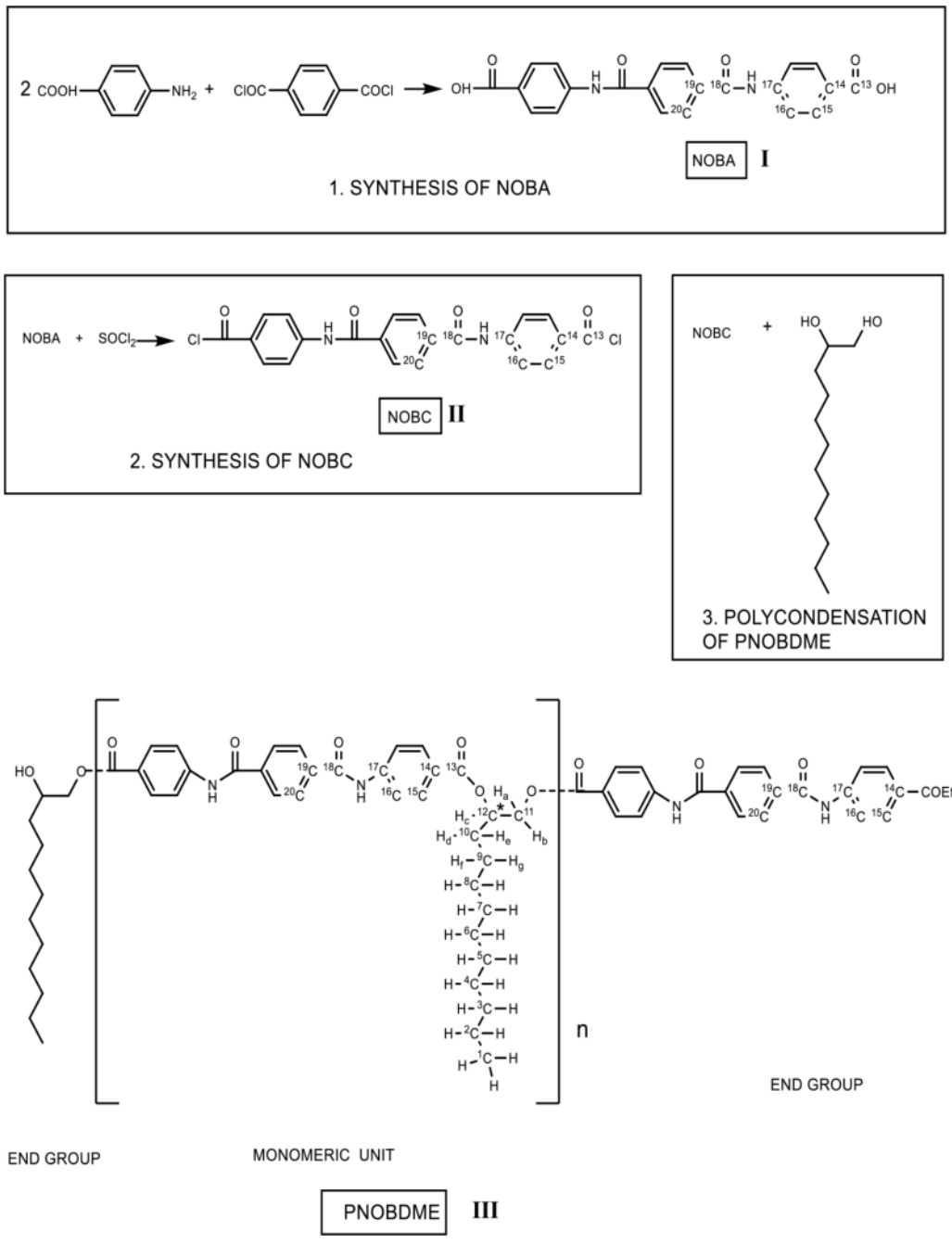

Figure 8.
Scheme of the synthetic way to attain PNOBDME.

The new cationic cholesteric LC polymers so designed were synthesized as follows: PTOBDME-choline $[(C_{34}H_{36}O_8)_n{-}C_5H_{13}N]$; PTOBEE-choline $[(C_{26}H_{20}O_8)_n{-}C_5H_{13}N]$; PTOBDME-ammonium $[(C_{34}H_{36}O_8)_n{-}C_5H_{13}N]$; PTOBEE-ammonium $[(C_{26}H_{20}O_8)_n{-}C_5H_{13}N]$; PTOBUME-amide $[(C_{33}H_{33}O_9N)_n]$; and PTOBEE-amide $(C_{26}H_{19}O_9N)_n$ [29].

These cationic polymers proved to be biocompatible, able to form polyplexes and capable of successfully condensing and transfecting the DNA into the nucleus cell, protecting DNA from inactivation by blood components. The complexes are sensitive to pH changes, possessing substantial buffering capacity below physiological pH. Their efficiency relies on extensive endosome swelling and rupture that provides an escape mechanism for the polycation/DNA complexes [30].

Since we are mainly interested in the design and chemical modifications of multifunctional cholesteric LC polyesters involving new properties but holding the precursor helical macromolecular structure, new cationic functionalization is held by introducing amide groups *para*-substituting the two ester groups in the central benzene ring of the terephthalate unit, along the main chain [31].

The final formulations of the new monomers, called PNOBDME and PNOBEE, are shown in **Figure 7(a)** and **(b)**, respectively. The hydrogen and carbon atoms have been numbered as precursors PTOBDME [16, 17] and PTOBEE [11, 15], respectively.

The synthetic way is based on our previous experience for the attainment of cholesteric LC polyesters and the condensation reaction reported by Sek et al. to obtain polyesteramides [32]. The intermediate acid chloride yield obtained here is lower than the precursor polyesters obtained. The synthetic way of polyesteramides PNOBDME $[C_{34}H_{38}N_2O_6]_n$ and PNOBEE $(C_{26}H_{22}N_2O_6)_n$ is given in **Figures 8** and **9**.

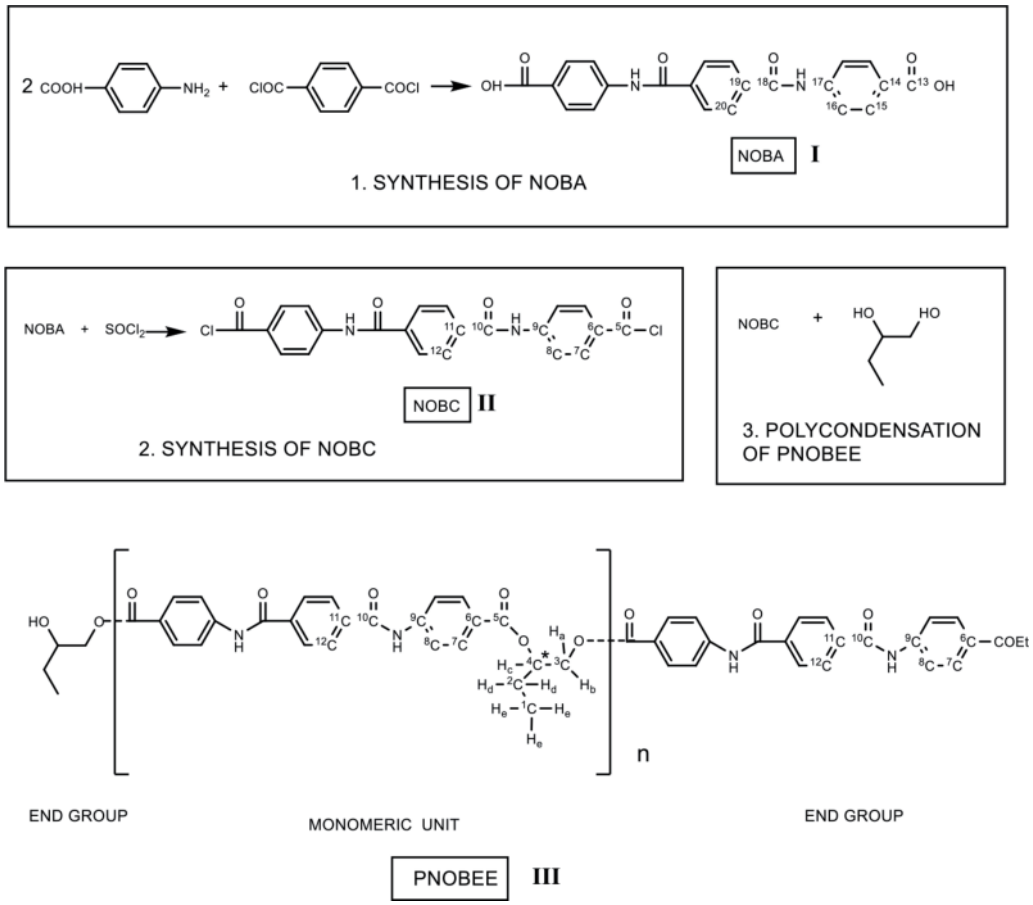

Figure 9.
Scheme of the synthesis of PNOBEE.

The structure of the polymers so obtained could be confirmed by ^{1}H, ^{13}C, COSY and HSQC NMR [31]. The NMR shifts were assigned according to our previous notation. Their thermal stability is studied by thermogravimetric (TG) and differential scanning calorimetry (DSC) analysis.

2. Experimental

2.1 Materials

2.1.1 Synthesis of PNOBDME {Poly[oxy(1,2-dodecane)-oxy-carbonyl-1,4-phenylene-amine-carbonyl-1,4-phenylene-carbonyl-amine-1,4-phenylene-carbonyl]}, $(C_{34}H_{38}N_2O_6)_n$

PNOBDME (III in **Figure 8**) was obtained through condensation reaction between 4, 4′-(terephthaloyl-diaminedibenzoic chloride) (NOBC) (II in **Figure 8**) and the racemic mixture of DL-1,2-dodecanediol. Similar notation to precursor cholesteric liquid crystal PTOBDME [16, 17] obtained by a similar method has been used.

2.1.1.1 Preparation of NOBA

Solutions of 0.1 mol terephthaloyl chloride in 200 ml carbon tetrachloride and 0.2 mol NaOH in water were added while stirring at room temperature for 15 min to a solution of 0.22 mol of 4-aminobenzoic acid and 0.2 mol NaOH in 400 ml water (Milli-Q grade) (4–4′-(terephthaloyl-diaminedibenzoic acid)) (NOBA), (I in **Figure 8**). Stirring was continued for 12 hours. Sediment was separated, filtered, washed several times with 40 ml of cold water, dried, comminuted and transferred to a vessel where it was mixed for 3 hours with 300 ml of hydrochloric acid. The product was filtered, washed several times with 40 ml of cold water, dried and comminuted. Yield is 28 g (70%).

2.1.1.2 Preparation of NOBC

In the course of 25 min, 15 g NOBA was added to 350 ml thionyl chloride, while stirring rapidly at room temperature (4- 4′-(terephthaloyl-diaminedibenzoic chloride)) (NOBC) (II in **Figure 8**). The solution was boiled with the reflux condenser. When the release of HCl ended and most of the sediment had dissolved, the hot solution was filtered and cooled down to 0°C for a day. The obtained product was separated, filtered, vacuum dried and recrystallized in chloroform. Yield is 7.2 g (48%).

2.1.1.3 Preparation of PNOBDME

A mixture of 0.017 mol NOBC and 0.017 mol DL-1,2-dodecanediol was added to 44 ml of diphenyl oxide. Purge with dry nitrogen was used for 25 min at room temperature, and then, while maintaining the gas current, the flask was transferred to a bath containing a high-temperature heat-transfer agent. The polycondensation was carried out for 3 hours and 30 min at 200°C. The reaction finished when the liberation of HCl ended. The result of the polycondensation reaction was poured into 500 ml of toluene, decanting PNOBDME, which was filtered, washed three times with ethanol and vacuum dried. The second fraction of PNOBDME precipitated of the filtrated toluene after 22 weeks was also filtered, washed with ethanol and vacuum dried. Yield first fraction is 2.6 g (25.5%); yield first and second fraction is 3.1 g (30.4%).

2.1.2 Synthesis of PNOBEE {Poly[oxy(1,2-butylene)-oxy-carbonyl-1,4-phenylene-amine-carbonyl-1,4-phenylene-carbonyl-amine-1,4-phenylene-carbonyl]}: $(C_{26}H_{22}N_2O_6)_n$

PNOBEE (III in **Figure 9**) was obtained through condensation reaction between (4- 4′-(terephthaloyl-diaminedibenzoic chloride)) (NOBC) (II in **Figure 9**) and the racemic mixture of DL-1,2-butanediol. Notation of cholesteric liquid crystal precursor PTOBEE has been used.

NOBC was synthesized by the reaction between NOBA, (4–4′-(terephthaloyl-diaminedibenzoic acid)) (NOBA) (I in **Figure 9**), and $SOCl_2$ and recrystallized in chloroform; previously NOBA was obtained by interface condensation between terephthaloyl chloride and 4-aminobenzoic acid.

2.1.2.1 Preparation of PNOBEE

A mixture of 0.015 mol NOBC and 0.015 mol DL-1,2-butanediol was added to 39 ml of chloronaphthalene. Purge with dry nitrogen was used for 25 min at room temperature, and then, while maintaining the gas current, the flask was transferred to a bath containing a high-temperature heat-transfer agent. The polycondensation was carried out for 180 min at 200°C. The reaction finished when the liberation of HCl ended. The result of the polycondensation reaction was poured into 500 ml of toluene, decanting PNOBEE, which was filtered, washed with ethanol and vacuum dried. The second fraction of PNOBEE precipitated of the filtrated toluene after 22 weeks which was also filtered, washed with ethanol and vacuum dried. Yield is 2.9 g (46.5%).

The structures of NOBA and NOBC were confirmed by ^{1}H-RMN, ^{13}C-NMR, COSY, TOCSY, NOESY and HSQC registered in DMSO-d_6 at 25°C in a Bruker 300 MHz NMR spectrometer. The structure of PNOBDME was studied by ^{1}H-RMN, ^{13}C-NMR, COSY and HSQC, obtained in VARIAN 400 MHz and 500 MHz spectrometers, also at room temperature [31].

2.1.2.2 Starting materials

Terephthaloyl chloride from Sigma-Aldrich Chemie GmBH (Steinheim, Germany); carbon tetrachloride from Panreac Química (Montcada i Rexach, Barcelona, Spain); NaOH from Panreac Química (Montcada i Rexach, Barcelona, Spain); 4-aminobenzoic acid from Sigma-Aldrich Chemie GmBH (Steinheim, Germany); hydrochloric acid from Normapur VWR International (Fontenay-sous-Bois, France); thionyl chloride from Sigma-Aldrich Chemie GmBH (Steinheim, Germany); chloroform from SDS Votre Partenaire Chimie (Peypin, France); DL-1,2-dodecanediol from Fluka Chemie GmBH (Buchs, Switzerland); diphenyl oxide from Sigma-Aldrich Chemie GmBH (Steinheim, Germany); nitrogen from Praxair (Madrid, Spain); toluene from Merck KGaA (Darmstadt, Germany).

DL-1,2-butanediol from Fluka Chemie GmBH (Buchs, Switzerland); chloronaphthalene from Sigma-Aldrich Chemie GmBH (Steinheim, Germany).

The solvent used in NMR for all cases was DMSO-d_6 from Merck KGaA (Darmstadt, Germany) and DMSO for optical rotatory dispersion (ORD), from Scharlau Chemie.

3. Characterization techniques

Thermal stability was studied on a Mettler TA4000-TG50 at a heating rate of 10°C/min with nitrogen purge between 30 and 600°C. Thermal behaviour was

analyzed by DSC in a Mettler TA4000/DSC30/TC11 calorimeter, with a series of heating/cooling cycles in a temperature range between 0 and 230°C.

Microcalorimetry was estimated in a MicroCal Inc., model MCS-DSC, within a range of temperature 4–120°C, at a heating rate of 10–20°C/h, and a volume of sample 1.5 ml.

Optical rotatory dispersion was measured in a Perkin Elmer 241 MC polarimeter, at 25°C in DMSO. Conditions used: λ_{Na} = 589 nm, slit = 5 mm, integration time = 50 s; λ_{Hg} = 574 nm, slit = 14 mm, integration time = 50 s; λ_{Hg} = 546 nm, slit = 30 mm, integration time = 50 s; λ_{Hg} = 435 nm, slit = 5 mm, integration time = 50 s; and λ_{Hg} = 365 nm, slit = 2.5 mm, integration time = 50 s.

Morphology was evaluated in an environmental scanning electron microscope (ESEM), PHILIPS XL30.

Simultaneous SAXS/WAXS of PNOBDME were performed at 16.1.1 beamline of the synchrotron radiation source (SRS) at Daresbury Laboratory, Warrington, UK, with a monochromatized beam (λ = 1.4 Å). Both WAXS and SAXS detectors were lineal. HDPE was used to calibrate the WAXS data and wet collagen (rat tail tendon, d = 676.08 Å) to calibrate the q-axis of the SAXS detector ($q = 4\pi \sin \theta/\lambda$), where the scattering angle is defined by 2θ. The experimental data were corrected for background scattering, sample absorption and positional lack of linearity of the detector, with the help of ATSAS [23, 24]. The samples dispersed in dichloromethane solution were applied dropwise on the sample holder and the solvent let to evaporate.

3.1 Thermal behaviour of PNOBDME and PNOBEE

Figure 10(a) shows the thermogravimetric curve of polyesteramide PNOBDME first fraction. A 5 and 10% weight loss is observed, respectively, at 282 and 310.3°C, increasing the thermal stability range of precursor polyester PTOBDME, with 10% weight loss percentage at 280°C [16].

In **Figure 10(b)**, the PNOBEE thermal stability can be observed. A 10% weight loss is registered at 330°C, due to thermal decomposition, a value higher than those observed for PTOBEE (280°C) [11] and PNOBDME (310.3°C). The entrance of the amide group in the mesogen causes an increase of thermal stability with respect to PTOBEE.

In **Figure 11(a)**, the DSC analysis of PNOBDME first fraction is exhibited and its Microcalorimetry curve appears in **Figure 11(b)**.

During the first heating run of the DSC of PNOBDME, performed at 10°C/min rate, **Figure 11(a)**, a glass transition around 62.5°C is observed, together with a

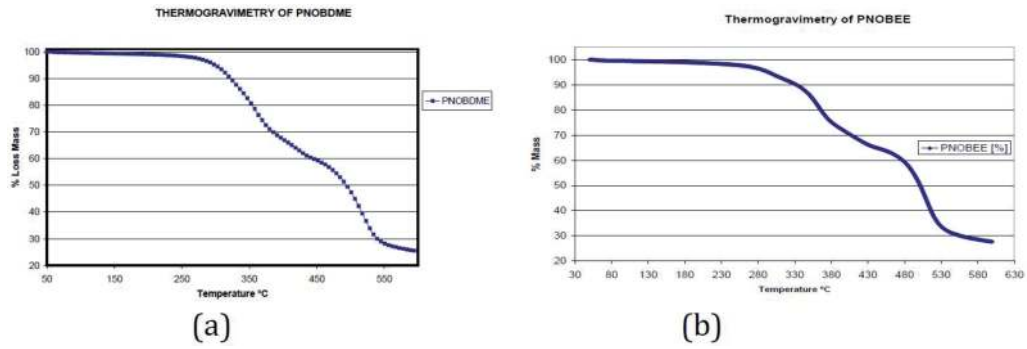

Figure 10.
(a) Thermogravimetric curve of PNOBDME first fraction; (b) thermogravimetric curve of PNOBEE first fraction.

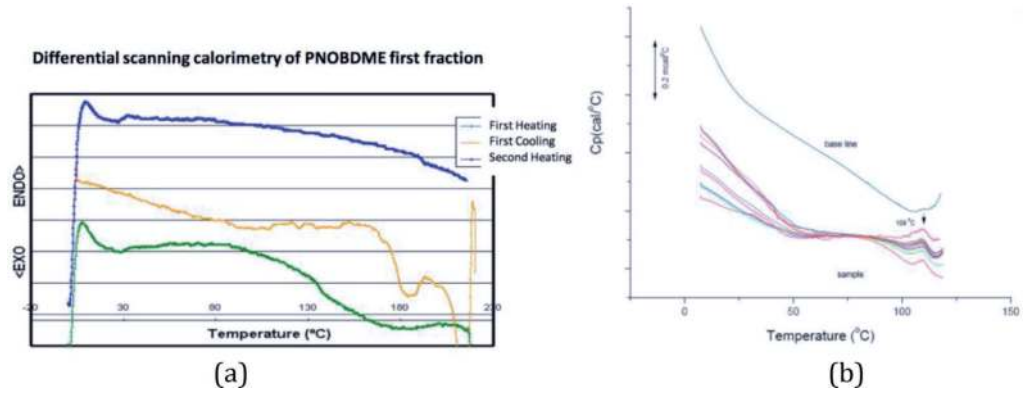

Figure 11.
(a) DSC analysis of PNOBDME first fraction; (b) microcalorimetry of PNOBDME.

small broad endothermic peak centred at 156°C. During the cooling, an exothermic peak at 183°C is indicative of crystallization from the mesophase, a higher value than that of PTOBDME (149°C). In the second heating, a glass transition is observed around 71.6°C and two broad and small endothermic peaks at 108.7 and 188.3°C.

Subsequently, PNOBDME was heated up to 230°C, at 10°C/min, cooled to 190°C and isothermally heated for 2 hours, then cooled to 30°C at 10°C/min and finally heated again to 230°C, at 10°C/min. Although the isothermal treatment at 190°C, after cooling from 230°C, should have produced an induced crystallization process (endothermic peak due to the polymer transition to mesophase), only a small endothermic peak at 109°C is observed not caused by the isothermal cooling. The endothermic transition from crystal to mesophase was also confirmed at 109°C by microcalorimetry, **Figure 11(b)**.

The DSC curve of PNOBEE is shown in **Figure 12**. During the first heating run (a), at a 10°C/min rate, a glass transition around 55°C is observed. A very broad endothermic peak centred at 185.3°C is interpreted as a fusion associated with a transition from crystal to liquid crystal. Another endothermic peak at 233.7°C is observed near the beginning of thermal decomposition. In the cooling run (b), two small exothermic peaks observed at 205.6 and 183.0°C are interpreted as crystallization processes from the mesophase. In the second heating (c), no transition is observed.

Compared to PTOBEE, with a transition to mesophase at 150°C and with exothermic crystal formation at 110°C during isothermal heating, a remarkable difference is observed by the substitution of ester groups by amide in the mesogen, increasing the stability range.

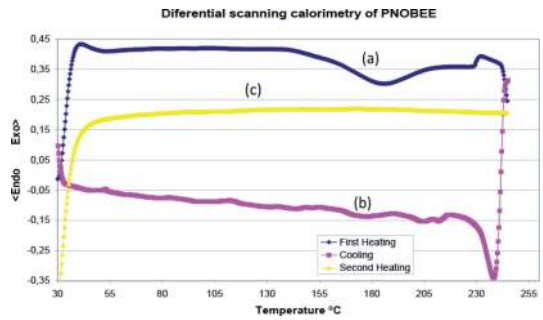

Figure 12.
DSC analysis of PNOBEE first fraction. (a) First heating run of the original sample; (b) subsequent cooling down; (c) second heating run.

3.2 Morphology of PNOBDME

The morphology of powdered PNOBDME without any previous treatment has been studied by SEM. In **Figure 13**, six details of the powder sample (a to f) are shown of the homogeneous spherical clusters of about 5 μm in diameter homogeneously dispersed.

3.3 Optical activity

Although synthesized from starting racemic materials, PNOBDME showed unexpected chirality. The first fraction of the polymer did not show a net optical activity but values fluctuated from positive to negative, but the second fraction presented a low but constant value +1.02°, at 598 nm; +1.65°, at 579 nm; and +2.9°, at 435 nm and a very high optical activity value between +600° and +950°, at 365 nm, depending on temperature. The same behaviour had been also observed in PTOBDME and PTOBEE.

The variation of the optical rotatory dispersion values (α) by the effect of time of the second fraction of PNOBDME is expressed in **Figure 14** as molar optical rotation $[\Phi] = [\alpha]\, M/100$, at 365 nm, at two different temperatures, 35°C and 25°C, being M the molecular weight of the polymer repeating unit.

At 35°C, the ORD of PNOBDME increases with time to a value approximate of 600°, preserved between 90 and 180 min. After that, it increases again to reach a value of 950°, getting stabilized after 360 min. After 120 min at 25°C, the ORD reaches a value of 600° conserved up to 9 hours.

In both cases, once the ORD value was stabilized to 600° and 950°, if the wavelength of the lamp changed from 365 to 435 nm and quickly returned to 365 nm, the ORD value initially decreased to +8.6 but recovered its value. This phenomenon is being reversible. The variation of ORD with time has been described in helical polyguanidines synthesized either from chiral monomers or from achiral monomers with chiral catalysts [33–39]. At the end of this article, the optical activity of PNOBEE has not been studied.

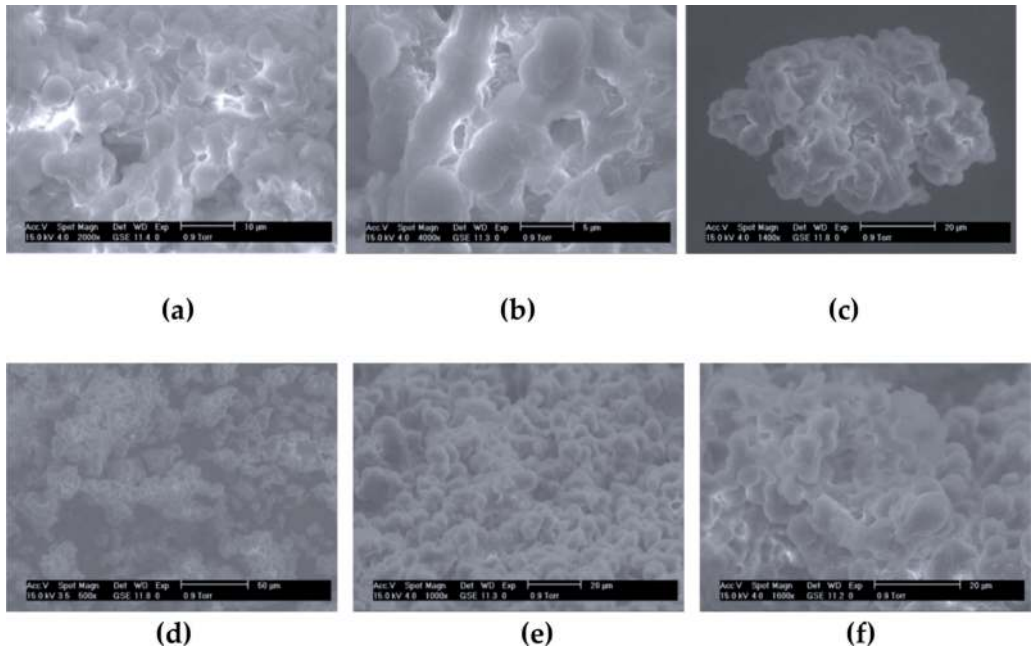

Figure 13.
SEM images of powdered PNOBDME.

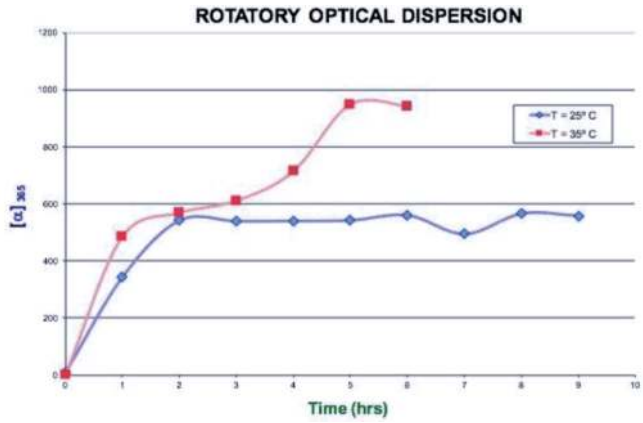

Figure 14.
Optical rotatory dispersion of PNOBDME second fraction at 25C and 35°C.

3.4 Molecular mechanics simulation of PNOBDME.

The structural fragment including a chiral secondary alcohol and a primary alcohol group (a beta-chiral 1,2-diol) is particularly interesting since it is present in many relevant natural products, such as sugars, nucleosides, glycerides [40], chiral nanostructures from helical polymers and metallic salts [41].

In the case of PNOBDME, the fragment in the spacer including the secondary alcohol group, bonded to chiral $^{12}C^*$, and the primary alcohol, bonded to prochiral ^{11}C, is shown in **Figure 15** for the R enantiomer of $^{12}C^*$.

Molecular mechanics always predict helical macromolecular structures along the main chain for PNOBDME and PNOBEE, as formulated in **Figure 7**. Instead, no helical polymer models were attained in the computational calculations when the amide group enters along the lateral side chains.

Molecular mechanics modeling was performed for the PNOBDME monomer with Materials Studio Windows v. 2019 [42]. COMPASS-II force field was loaded, including both atomic mass and charge. A model of the monomer is shown in **Figure 16(a)**, with optimized geometry to a minimum of energy, -95 Kcal/mol. Monomer polymerization was simulated by defining the ^{11}C atom as the *head atom,* within the *repeating unit*, and the O atom bonded to ^{13}'C, as the *tail atom*, being $^{12}C^*$ the chiral centre. Homopolymerization was then simulated with head-to-tail orientation and torsion angle between monomers fixed to 180°. Isotacticity was finally imposed on the polymer chain. The helical polymer model so obtained along the main chain is shown in **Figure 16(b)**. The perpendicular cross-section appears in **Figure 16(c)**.

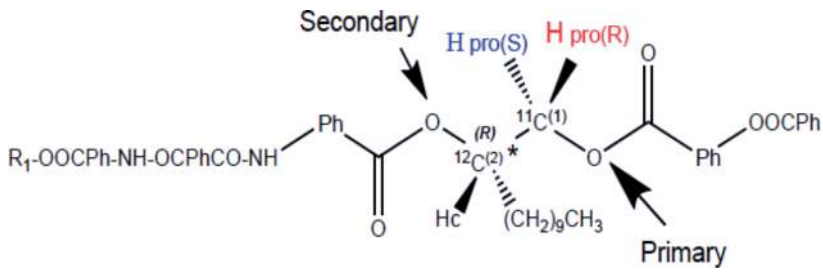

Figure 15.
Scheme of the spacer of PNOBDME including the two alcohol groups.

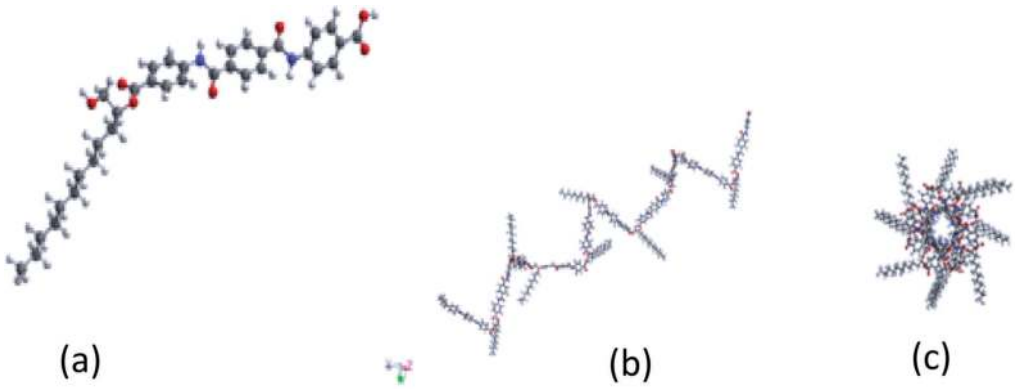

Figure 16.
Molecular simulation of PNOBDME monomer: (a) minimum energy MM model; (b) isotactic [PNOBDME]$_{10}$; (c) cross-sectional view.

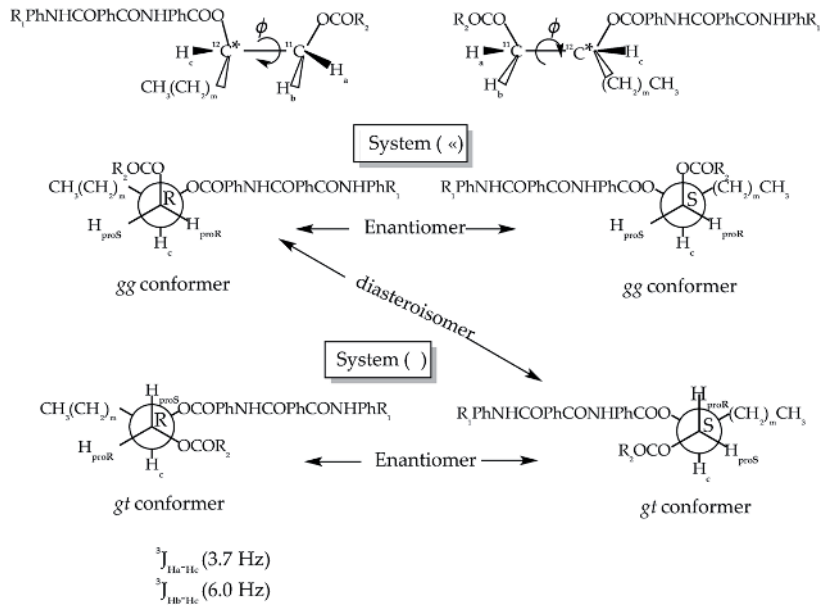

Figure 17.
The relationship between the four helical diastereomers gg and gt of the R and S enantiomers of PNOBDME and PNOBEE through the ^{11}C–$^{12}C^*$ bond, and ^3C–$^4C^*$ (torsion φ), respectively.

3.5 Conformational analysis of PNOBDME and PNOBEE

The tetrahedral carbon atoms **11C** in PNOBDME, allocated in *α* with respect to the asymmetric carbon atom $^{12}C^*$ (**Figure 7(a)** with m = 9) and **3C** in PNOBEE, allocated in *α* with respect to chiral $^4C^*$ (**Figure 7(b)** with m = 1), along the polymer backbones, are referred as *prochirals*, since both could be converted into a chiral centre by arbitrarily changing only one attached H group to a deuterium atom (D with higher priority than H). Depending on the configuration, R/S, of the so created chiral centre, the H atom ideally deuterated, would be labeled as *pro-R/S*.

The two hydrogen atoms on the *prochiral ^{11}C carbon atom*, H_a and H_b, in PNOBDME, can be described as *prochiral hydrogens*. Prochiral hydrogens can be also designated as *diastereotopic*. Their indistinguishable signals by ^{1}H-NMR split then into two signals easily differentiated. The same effect is observed for H_d and H_e, bonded to prochiral ^{10}C, and for H_f and H_g, bonded to prochiral ^9C.

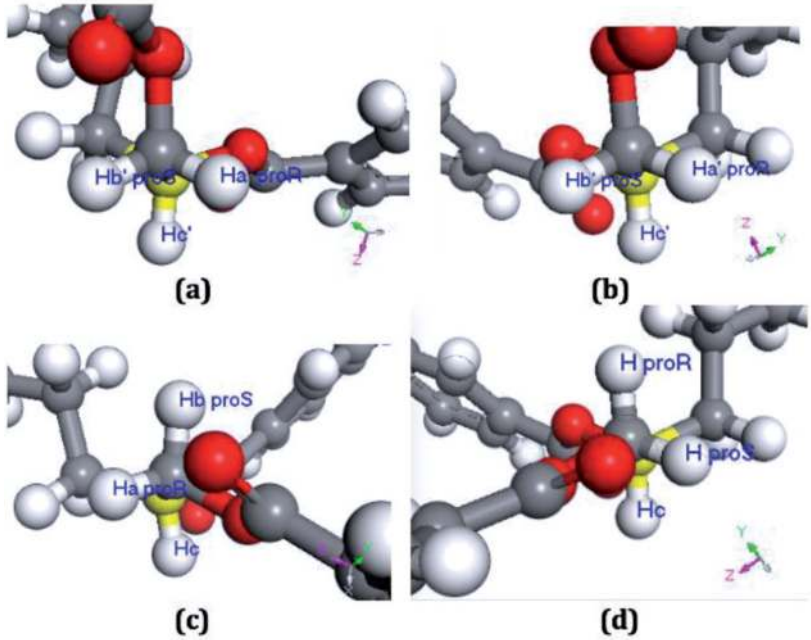

Figure 18.
Molecular model details of a PNOBDME dimer. View along ^{11}C–$^{12}C^*$ bond (perpendicular to the paper), with (R) and (S) absolute configuration of $^{12}C^*$ (in yellow behind ^{11}C) for (a) Rgg-diasteroisomer; (b) Sgg-diasteroisomer; (c) Rgt-diasteroisomer; (d) Sgt diasteroisomer.

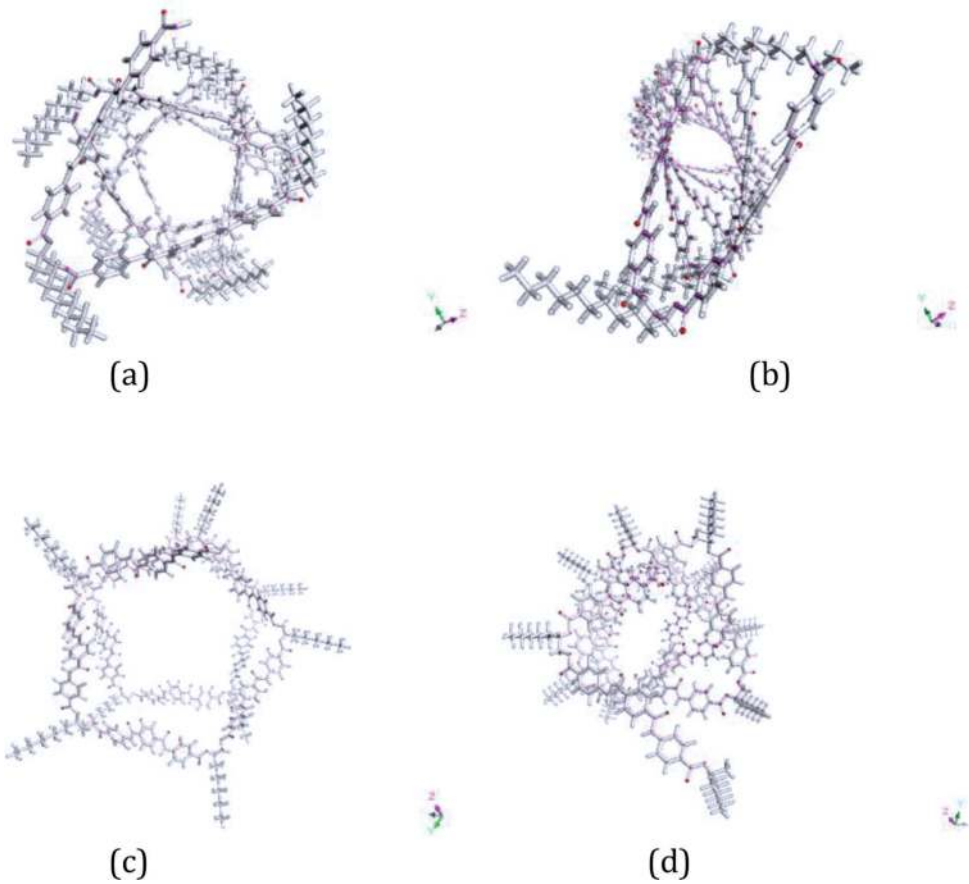

Figure 19.
Molecular model details of PNOBDME polymers: (a) Poly10_PNOBDME_Rgg; (b) Poly10_PNOBDME_Sgg; (c) Poly10_PNOBDME_Rgt; (d) Poly10_PNOBDME_Sgt.

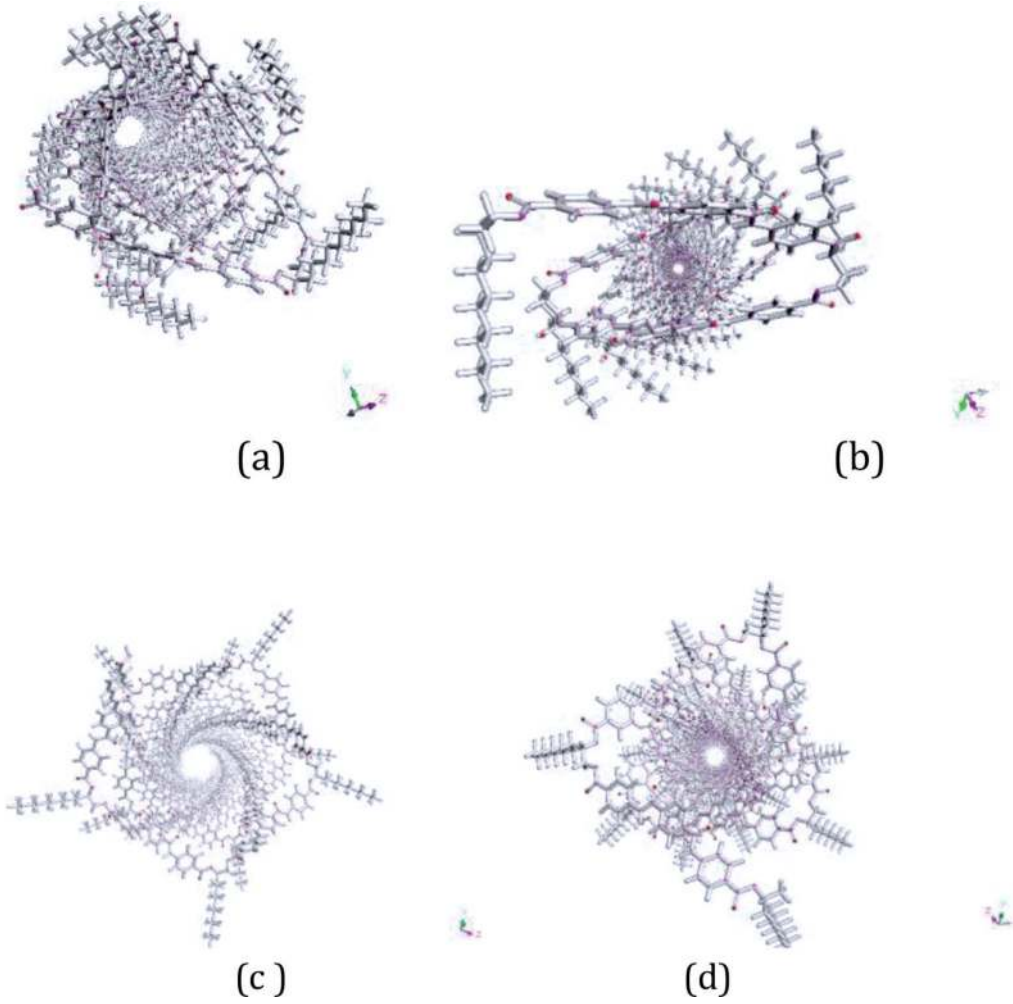

Figure 20.
Molecular model details of PNOBDME polymers: (a) Poly6o_PNOBDME_Rgg; Poly6o_PNOBDME_Sgg; (c) Poly6o_PNOBDME_Rgt; (d) Poly6o_PNOBDME_Sgt.

Equally the two hydrogen atoms on *prochiral ^{3}C carbon atom*, H_a and H_b, of PNOBEE, are considered as *prochiral hydrogens.*

Two independent sets of signals are experimentally observed by ^{1}H-NMR for each enantiomer of PNOBDME and PNOBEE [31]. They are related to the two possible staggered diastereomeric conformers, *gg* and *gt* of torsion φ along the $^{11}C–^{12}C^*$ bond in PNOBDME and $^{3}C–^{4}C^*$ in PNOBEE, along the polymer backbone. One of these two systems is designated with an apostrophe (') and the other is designed without an apostrophe ().

The combination of a helix with two screw senses and the two absolute configurations by the presence of the asymmetric carbon atom provides four diastereomeric structures. There are two pairs of enantiomers each with two independent sets of ^{1}H-NMR signals. The four diastereomers of PNOBDME are depicted in **Figure 17**.

The existence of two independent conformers had also been observed for each enantiomer of PTOBDME and PTOBEE. It was also related to the presence of helical structures, the Cotton effect and the sign of the helicity in the case of 1-2 di-O-benzoylated sn-glycerols [33–39].

Details of molecular models for *gg* and *gt* conformers of a dimer of PNOBDME are shown (**Figure 18**), projected along the $^{11}C–^{12}C^*$ bond and torsion φ

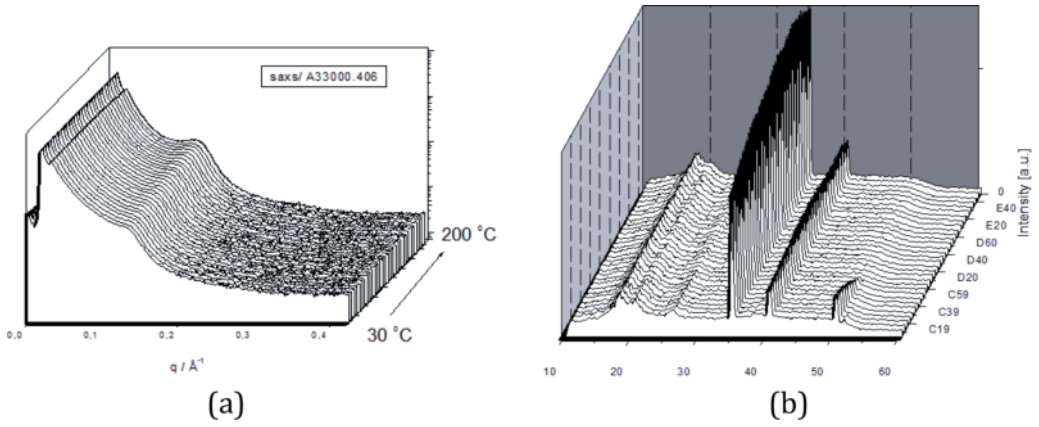

Figure 21.
Simultaneous SAXS (a)/WAXS (b) patterns of PNOBDME.

(perpendicular to the paper) with $^{12}C^*$ (bonded to H_c) having *R* and *S* absolute configuration, in yellow, behind ^{11}C (bonded to H_a and H_b).

Helical polyesteramide $(PNOBDME)_{10}$ molecular models obtained with the four diastereomers, after minimizing the corresponding monomers are described in **Figure 19**.

Polymer models with 60 monomers of the 4 are exhibited in **Figure 20**.

3.6 Simultaneous SAXS/WAXS of PNOBDME

Figure 21(a) and **(b)** shows the simultaneous SAXS/WAXS patterns of PNOBDME registered during heating from 30–200°C, with a synchrotron radiation source.

The SAXS spectra show two sharp order reflections at *q* value of 0.018 $Å^{-1}$ (55.5 Å) and 0.029 $Å^{-1}$ (34.48 Å).

Four WAXS peaks, at $2\theta \cong 18.39^{\circ}$ (d = 4.38 Å); 18.83° (d = 4.28 Å); 35.17 (d = 2.31 Å); and 40.75 (d = 2.01 Å) always remaining present in the entire temperature range, were assigned to the cholesteric mesophase.

Peaks at $2\theta \cong 26.39$ (d = 3.07 Å) and 50.71 (d = 1.73 Å) disappearing at about 90°C during the heating range are attributed to crystal 3D phase.

4. Conclusions

The synthetic multifunctional cholesteric liquid crystal polyesteramides designed as PNOBDME $(C_{34}H_{38}N_2O_6)_n$ and PNOBEE $(C_{26}H_{22}N_2O_6)_n$ are reported as chemical modifications of multifunctional cholesteric LC polyesters, involving new properties but holding the precursor helical macromolecular structure.

Molecular mechanics models of the new polymers show helical polymeric rigid chains. Homopolymerization was simulated with head-to-tail orientation and torsion angle between monomers fixed to 180°. Isotacticity was finally imposed on the polymer chains, explained in terms of the higher reactivity of the primary hydroxyl regarding the secondary one in the glycol through the polycondensation reaction.

Two independent sets of signals experimentally observed by ^1H-NMR for each enantiomer of PNOBDME and PNOBEE (while the R/S ratio of asymmetric carbon atoms remained 50:50) are related with two possible staggered diastereomeric conformers, *gg* and *gt* of torsion φ, containing the asymmetric carbon atom in the spacer, along the polymer backbone. One of these two systems is designated with an

apostrophe ('), and the other is designed without an apostrophe (). The combination of a helix with two screw senses and the two absolute configurations by the presence of the asymmetric carbon atom provides four diastereomeric structures.

Molecular models of the four diastereomers *Rgg*, *Sgg*, *Rgt* and *Sgt* are provided as well as their polymer chains with 10 and 60 monomeric units.

The thermal behaviour of the new synthesized cholesteric liquid crystal polyesteramides has been studied by TG and DSC. An endothermic peak assigned to the first-order transition from crystal to liquid crystal mesophase is observed in both polymers.

ORD values are provided for polyesteramide PNOBDME. The first fraction of the polymer did not show a net optical activity but values fluctuating from positive to negative, but the second fraction presented low positive values +1.02°, at 598 nm; +1.65°, at 579 nm; and +2.9°, at 435 nm but very high optical activity +600° to +950°, at 579 nm, when increasing temperature from 25–35°C.

Morphology of powdered PNOBDME by ESEM shows spherical clusters of about 5 μm in diameter, homogeneously dispersed.

Simultaneous SAXS/WAXS patterns of PNOBDME are registered during heating from 30 to 200°C, with a synchrotron radiation source.

Acknowledgements

We thank CSIC for their facilities. We acknowledge support of the publication fee by the CSIC Open Access Publication Support Initiative through its Unit of Information Resources for Research (URICI).

Author details

Mercedes Pérez Méndez[1*] and José Fayos Alcañiz[2]

1 Instituto de Ciencia y Tecnologia de Polimeros (CSIC), Madrid, Spain

2 Instituto de Química Física Rocasolano (CSIC), Madrid, Spain

*Address all correspondence to: perezmendez@ictp.csic.es

References

[1] Schrödinger E. What Is Life? The Physical Aspect of the Living Cell. New York: Cambridge University Press; 1945

[2] Macías Barber E. El cristal aperiódico de la vida. Revista de la Unión Iberoamericana de la Sociedad de Física. 2006;**2**:7-16

[3] Franklin RE, Goslin RG. Molecular configuration in sodium thymonucleate. Nature. 1953;**171**:740-741

[4] Watson JD, Crick FHC. Molecular structure of nucleic acids: A structure for deoxyribose nucleic acid. Nature. 1953;**171**:737-738

[5] Wilkins MHF, Stokes AR, Wilson HR. Molecular structure of deoxypentose nucleic acids. Nature. 1953;**171**:738-740

[6] Ringsdorf H, Schlarb B, Venzmer J. Molecular architecture and function of polymeric oriented systems: Models for the study of organization, surface recognition, and dynamics of biomembranes. Angewandte Chemie (International Ed. in English). 1988;**27**:113

[7] International Union of Crystallography. Report of the Executive Committee for 1991. Acta Crystallographica. 1992;**A48**:922

[8] Zanchetta G. Liquid crystalline phases in oligonucleotide solutions [thesis]. University of Milan; 2007

[9] Kornyshev AA, Leikin S, Malinin SV. Chiral electrostatic interaction and cholesteric liquid crystals of DNA. European Physical Journal E: Soft Matter and Biological Physics. 2002;**7**:83-93

[10] Lai SL, Hartono D, Yang K-L. Self-assembly of cholesterol DNA at liquid crystal/aqueous interface and its application for DNA detection. Applied Physics Letters. 2009;**95**:153702

[11] Pérez-Méndez M, Marco C. New synthesis, thermal properties and texture of cholesteric poly[ethyl ethylene 4,4′-(terephthaloyldioxy)dibenzoate]. Acta Polymerica. 1997;**48**:502-506

[12] Pérez-Méndez M, Marco Rocha C. Preparing cholesteric liquid-crystals - by adding acid dichloride and butanediol to chloro-naphthalene, heating in nitrogen, decanting into toluene, etc. Patent family: Patent with no. EP1004650-A; WO9831771-A; WO9831771-A1; AU9854863-A; ES2125818-A1; ES2125818-B1; EP1004650-A1; US6165382-A; MX9906732-A1; JP2001513827-W; AU739076-B; EP1004650-B1; DE69824182-E

[13] Bilibin AY, Ten'kovtsev AV, Piraner ON, Skorokhodov SS. Synthesis of high molecular weight liquid crystal polyesters based on a polycondensation mesogenic monomer. Polymer Science U.S.S.R. 1984;**26**(12):2882-2890

[14] Bilibin AY, Skorokhodov SS. Rational path of the synthesis of liquid-crystalline high molecular weight polyesters and their properties in solution. Macromolecular Symposia. 1989;**29**:9-23

[15] Perez-Mendez M, Marsal R, Garrido L, Martin-Pastor M. Self-association and stereoselectivity in a chiral liquid-crystal cholesteric polymer formed under achiral conditions. Macromolecules. 2003;**36**:8049-8055

[16] Fayos J, Sánchez-Cortés S, Marco C, Pérez-Méndez M. Conformational analysis and molecular modeling of cholesteric liquid-crystal polyesters based on XRD, Raman and transition thermal analysis. Journal of Macromolecular Science, Physics. 2001;**B40**(3&4):553-576

[17] Pérez Méndez M, Sanguino J. Cholesteric liquid-crystal copolyester,

poly[oxycarbonyl-1,4-phenylene-oxy –1,4 terephthaloyl- oxy-1,4-phenylene- carbonyloxy (1,2-dodecane)] [C34H36O8]n, synthesized from racemic materials: Kinetics, structure and optical characterization. Journal of Engineering Research and Applications. 2015;**5**(7, (Part-2)):48-62

[18] Boiko N, Shibaev V. Cholesteric polymer liquid crystals and their optical properties. International Journal of Polymeric Materials. 2000;**45**(3-4):533-583

[19] Sánchez-CortésS,Marsal-BerenguelR, Pérez-Méndez M. Adsorption of a cholesteric liquid-crystal polyester on silver and gold nanoparticles and films studied by surface-enhanced Raman scattering. Applied Spectroscopy. 2004;**58**(5):562-569

[20] Pérez-Méndez M, Fayos J, Mateo CR. Chapter 24: Self-assembly of cholesteric liquid-crystal polyesters and their stereoselective interaction with liposomes of DMPC. In: Pályi G, Zucchi C, Caglioti L, editors. Advances in Biochirality. Oxford, UK: Elsevier Science Ltd.; 1999

[21] Pérez-Méndez M, Areso S, Alarcón Vaquero A, Elorza B, Malfois M. Effect of polymer addition to lipid membranes as potential drug delivery systems. Structure and dynamics of their interaction, Annual Report EMBL; 1998. p. 372

[22] Perez-Mendez M, Fayos J, Blanch GP, Sánchez Cortés S. Biofunctionalization of cholesteric liquid-crystal helical polymers. Nanocarriers. In: Nalwa HS, editor. Encyclopedia of Nanoscience and Nanotechnology. ACS. Valencia, California, USA: American Scientific Publishers. Vol. 11. 2011. pp. 547-580. ISBN: 1-58883-160-4

[23] Konarev PV, Petoukhov MV, Volkov VV, Svergun DI. ATSAS 2.1, a program package for small-angle scattering data analysis. Journal of Applied Crystallography. 2006;**39**(Part 2):277-286. DOI: 10.1107/S0021889806004699

[24] Kostorz G, Svergun DI, Koch MHJ, Timmins PA, May RP, editors. Small angle X-ray and neutron scattering from solutions of biological macromolecules. In: IUCr Texts on Crystallography; No. 19. Oxford University Press; 2013. p. 358. ISBN: 978-0-19-963953-3. Published to Oxford Scholarship Online: December 2013: DOI: 10.1093/acprof:oso/9780199639533.001.0001

[25] Anderson WF. Human gene therapy. Nature. 1998;**392**(6679 Suppl):25-30

[26] Ibraheem D, Elaissari A, Fessi H. Gene therapy and DNA delivery systems. International Journal of Pharmaceutics. 2014;**459**(1-2):70-83

[27] Pérez Méndez M, Marsal Berenguel R, Sánchez Cortés S. New non-viral vectors based on biocompatible liquid-crystal polymers for the carriage and delivery of biomacromolecules and insoluble drugs as a strategy. Revista de Oncología. 2002;**4**(Supl. 1):177

[28] Pérez Méndez M, Marsal Berenguel R, Funari SS. Structural characterization of the interaction between cholesteric liquid-crystal polymers and molecules of biological interest. HASYLAB Annual Report. 2003:11150. Available from: http://hasyweb.desy.de/science/annual_reports/2003_report/part1/contrib/47/11150.pdf

[29] Pérez Méndez M. Chapter 2: Synthetic cationic cholesteric liquid crystal polymers, liquid crystals. In: Choudhury PK, editor. Recent Advancements in Fundamental and Device Technologies. Rijeka: InTech Open; 2018. pp. 7-33. Available from: https://cdn.intechopen.com/pdfs-wm/58375.pdf

[30] Pérez Méndez M, Rodríguez Martínez D, Fayos J. Structure of non-viral vectors based on cholesteric liquid-crystal polymers by SAXS. International Journal of Advancement In Engineering Technology, Management and Applied Science (IJAETMAS). 2016;**03**(11):27-41. ISSN: 2349-3224

[31] Pérez Méndez M. Biocompatible, nanostructured, chiral polyesteramides: PNOBDME (C34H38N2O6)n and PNOBEE (C26H22N2O6)n synthesized and characterised as cholesteric liquid crystals. International Journal of Engineering Research and Applications (IJERA). 2019;**9**(6 (Part –1)):52-66. DOI: 10.9790/9622- 0906015267

[32] Sek D, Wolinska A, Janeczek H. Structure-liquid crystalline properties relationship of polyesteramides. Journal of Polymer Materials. 1986;**3**:225-233

[33] Uzawa H, Nishida Y, Ohrul H, Meguro H. Application of the dibenzoate chirality method to determine the absolute configuration of glycerols and related acyclic alcohols. The Journal of Organic Chemistry. 1990;**55**:116-122

[34] Ute K, Hirose K, Kashimoto H, Hatada K, Vogl O. Haloaldehyde polymers. 51. Helix-sense reversal of isotactic chloral oligomers in solution. Journal of the American Chemical Society. 1991;**113**:6305-6306. DOI: 10.1021/ja00016a076

[35] Ute K, Oka K, Okamoto Y, Hatada K, Xi F, Vogl O. Haloaldehyde polymers LIII. Optical resolution of purely isotactic oligomers of chloral: Optical activity of the chloral oligomers assuming one-handed helical conformation in solution. Polymer Journal. 1991;**23**:1419-1424

[36] Tian G, Lu Y, Novak BM. Helix-sense selective polymerization of carbodiimides: Building permanently optically active polymers from achiral monomers. Journal of the American Chemical Society. 2004;**126**:4082-4083

[37] Schlitzer DS, Novak BM. Trapped kinetic states, chiral amplification and molecular chaperoning in synthetic polymers: Chiral induction in Polyguanidines through ion pair interactions. Journal of the American Chemical Society. 1998;**120**(9):2196-2197

[38] Tang H-Z, Lu Y, Tian G, Capracotta MD, Novak BM. Stable helical polyguanidines: Poly{N-(1-anthryl)-N‘-[(R)-and/or (S)-3,7-dimethyloctyl]guanidines}. Journal of the American Chemical Society. 2004;**126**:3722-3723

[39] Muller M, Zentel R. Interplay of chiral side chains and helical Main chains in polyisocyanates. Macromolecules. 1996;**29**:1609-1617

[40] Freire F, Seco JM, Quiñoá E, Riguera R. The prediction of the absolute stereochemistry of primary and secondary 1,2-Diols by 1H NMR spectroscopy: Principles and applications. Chemistry–A European Journal. 2005;**11**(19):5509-5522

[41] Arias S, Freire F, Quiñoá E, Riguera R. Nanospheres, nanotubes, toroids, and gels with controlled macroscopic chirality. Angewandte Chemie International Edition. 2014;**53**(50):13720-13724

[42] Materials Studio Modeling v.2018, BIOVIA Cambridge, U.K. Inc.; 2018